NeuroImage: Clinical 37 (2023) 103334

Contents lists available at ScienceDirect

NeuroImage: Clinical

journal homepage: www.elsevier.com/locate/ynicl

Spinal cord motion assessed by phase-contrast MRI - An inter-center pooled data analysis

Katharina Wolf [a,*], Nikolai Pfender [b], Markus Hupp [b], Marco Reisert [c], Axel Krafft [c], Reto Sutter [d], Marc Hohenhaus [e], Horst Urbach [f], Mazda Farshad [g], Armin Curt [b]

[a] Department of Neurology and Neurophysiology, Medical Center, University of Freiburg, Faculty of Medicine, University of Freiburg, Germany
[b] Spinal Cord Injury Center, Balgrist University Hospital, University of Zurich, Zurich, Switzerland
[c] Department of Radiology, Medical Physics, Medical Center, University of Freiburg, Faculty of Medicine, University of Freiburg, Germany
[d] Radiology, Balgrist University Hospital, University of Zurich, Zurich, Switzerland
[e] Department of Neurosurgery, Medical Center, University of Freiburg, Faculty of Medicine, University of Freiburg, Germany
[f] Department of Neuroradiology, Medical Center, University of Freiburg, Faculty of Medicine, University of Freiburg, Germany
[g] University Spine Center Zurich, Balgrist University Hospital, University of Zurich, Zurich, Switzerland

A B S T R A C T

Background: Phase-contrast MRI of CSF and spinal cord dynamics has evolved among diseases caused by altered CSF volume (spontaneous intracranial hypotension, normal pressure hydrocephalus) and by altered CSF space (degenerative cervical myelopathy (DCM), Chiari malformation). While CSF seems to be an obvious target for possible diagnostic use, craniocaudal spinal cord motion analysis offers the benefit of fast and reliable assessments. It is driven by volume shifts between the intracranial and the intraspinal compartments (Monro-Kellie hypothesis). Despite promising initial reports, comparison of spinal cord motion data across different centers is challenged by reports of varying value, raising questions about the validity of the findings.
Objective: To systematically investigate inter-center differences between phase-contrast MRI data.
Methods: Age- and gender matched, retrospective, pooled-data analysis across two centers: cardiac-gated, sagittal phase-contrast MRI of the cervical spinal cord (segments C2/C3 to C7/T1) including healthy participants and DCM patients; comparison and analysis of different MRI sequences and processing techniques (manual versus fully automated).
Results: A genuine craniocaudal spinal cord motion pattern and an increased focal spinal cord motion among DCM patients were depicted by both MRI sequences ($p < 0.01$). Higher time-resolution resolved steeper and larger peaks, causing inter-center differences ($p < 0.01$). Comparison of different processing methods showed a high level of rating reliability (ICC > 0.86 at segments C2/C3 to C6/C7).
Discussion: Craniocaudal spinal cord motion is a genuine finding. Differences between values were attributed to time-resolution of the MRI sequences. Automated processing confers the benefit of unbiased and consistent analysis, while data did not reveal any superiority.

1. Introduction

Among diseases that are related to narrowed CSF space, such as degenerative cervical myelopathy (DCM) and Chiari I malformation, or altered CSF volume, such as spontaneous intracranial hypotension, idiopathic intracranial hypertension, and normal pressure hydrocephalus, non-invasive, spinal phase-contrast MRI may help to solve known clinical-anatomical ambiguities by providing in vivo diagnostics of CSF and CNS dynamics (Carroll and Callen, 2022; Hoxworth, 2014; Wymer et al., 2020; Kelly and Yamada, 2016; Bradley et al., 2016; Stöcklein et al., 2022). While qualitative measures of CSF flow are acknowledged as part of clinical routine diagnostics (normal pressure hydrocephalus, Chiari I malformation), quantitative analysis is challenged by fluid dynamics, such as bidirectional flow, turbulences, and multiform boundaries (Bunck et al., 2011). In contrast, craniocaudal motion of the spinal cord can be quantitatively and qualitatively measured (Hupp et al., 2019; Hupp et al., 2021; Wolf et al., 2021; Wolf et al., 2021; Wolf et al., 2022). It has the benefit of fast and reliable assessment, segmentation, and processing. Furthermore, the passive motion is driven by changes in blood volume *and* CSF volume (Cushing, 1925; Tain et al., 2011; Schmidt et al., 1968; Matsuzaki et al., 1996), thus reflecting information beyond CSF shifts, and the information gathered can be linked to CNS strain. (Wolf et al., 2021; Wolf et al., 2021) Spinal cord motion has been an upcoming target among recent studies mainly focusing on DCM:

Abbreviations: aMCC, adapted maximum canal compromise; CNN, convolutional neural network; DCM, degenerative cervical myelopathy; ICC, Intra-class Correlation Coefficient; ROI, region of interest; V_{ENC}, velocity encoding.

* Corresponding author at: Department of Neurology and Neurophysiology, Breisacher Str. 64, D-79106 Freiburg, Germany.
E-mail address: katharina.wolf@uniklinik-freiburg.de (K. Wolf).

https://doi.org/10.1016/j.nicl.2023.103334
Received 14 December 2022; Received in revised form 17 January 2023; Accepted 19 January 2023
Available online 23 January 2023

focally increased craniocaudal spinal cord motion has been described by axial and sagittal phase-contrast MRI acquisitions (Vavasour et al., 2013; Chank et al., 2014; Hupp et al., 2019; Hupp et al., 2021; Hupp et al., 2019) as well as ongoing strains across the cervical spinal cord, and prolonged motion over one heartbeat (Hupp et al., 2021; Wolf et al., 2021; Wolf et al., 2021). The "AO Spine RECODE-DCM" (aospine.org/recode) has addressed the well described functional – anatomical – paradox with ambiguous clinical and radiological presentations and has proposed a disease concept recognizing factors of dynamic stress on the spinal cord beyond the absolute anatomical extent of the stenosis (Davies et al., 2022).

Additionally, relevant increases of spinal cord motion at segment C2/C3 have also been depicted in patients with spontaneous intracranial hypotension and definite leak (Wolf et al., 2022), and decreased spinal cord motion in cases with idiopathic intracranial hypertension (Wolf et al., 2022) which is most likely caused by the loss, or the surplus of the surrounding resistances due to alterations in CSF volume, respectively.

Thus, spinal cord motion might be a promising, yet to be clinically evaluated target relating to changes of intracranial pressure. In DCM, focal analysis of spinal cord motion might possibly be enabling the prediction of those at risk of developing progressive myelopathy.

Despite reproduction of similar effects among the most recent studies on spinal cord motion in DCM (Hupp et al., 2021; Wolf et al., 2021; Hupp et al., 2019), the reported values differed by almost a factor of two (Supplement 1). As this factor lies beyond any expected variability, it is crucial to understand these differences and to explore intermodal comparability before proceeding with further trials.

Some technical details on phase-contrast MRI and processing might be of importance: e.g., the sensitivity to different velocities depends on the pre-determined velocity encoding (V_{ENC}) gradient. If the chosen V_{ENC} is too high, measurements are insensitive to low velocities; if the chosen V_{ENC} is too low, high velocities cannot be measured (Wymer et al., 2020; Johnson and Markl, 2010; Markl, 2022). These extreme values appear as so-called phase-wraps, or aliasing artifacts. To a limited extent, aliasing can be corrected (Herráez et al., 2002; Kasim, 2017). Also, a higher V_{ENC} might cause a slightly higher range of data variability (Lotz et al., 2002). Additionally, an effect called phase-drift might lead to an offset-error of the velocity measurements, that results in a systematic overestimation of each value. It can be systematically corrected by different methods (Wymer et al., 2020; Johnson and Markl, 2010). Time-resolution and different standards of data processing might play a role (Lotz et al., 2002).

It therefore could be hypothesized, that overestimation of spinal cord motion might be due to incorrect segmentation and/or data processing; underestimation might be due to lower time-resolution and/or low V_{ENC} without correction of phase-wraps.

The aim of this study was to systematically explore differences between MRI protocols and data processing methods across centers and their effect upon possible confounding factors.

2. Methods

Study outline: retrospective, inter-center pooled-data analysis of healthy participants and DCM patients that had been included within separate, prospective studies. Data had been collected between July 2016 and February 2020 (Center 1) and between June 2018 to February 2021 (Center 2). Written informed consent of each participant was obtained. The local ethic committees approved to the trials (Vote numbers: Center 1: KEK-ZH 2012-0343, BASEC Nr. PB_2016-00623, registered at https://www.clinicaltrials.gov – NCT 02170155; Center 2: EK-FR 261/17, EK-FR 338/17, registered at German registry of clinical trials, DRKS00017351, DRKS00012962).

Recruitment procedures, inclusion and exclusion criteria have been reported by each center (Hupp et al., 2019, 2021; Wolf et al., 2019; Wolf et al., 2021). In short: healthy participants were required to have no impairment in daily life and no incidental relevant stenosis in the latter MRI; DCM patients were required to present with symptomatic relevant cervical stenosis. Mild symptoms beyond radiculopathy as clumsiness of hands, or loss of dexterity were accepted. At Center 2, only monosegmental relevant stenosis was included.

Selection of datasets:

Datasets of all healthy participants and DCM patients at Center 1 were screened and included if there were no typical MRI artifacts, and if T2-weighted images could be used as an overlay on phase-contrast images. DCM patients were additionally required to present with monosegmental stenosis. Included datasets were matched 1:1 by age, sex, and level of stenosis (if applicable) to a cohort of Center 2 for inter-center comparison. For comparison of different processing methods, repeated measurements of healthy participants at Center 1 were included as well, if they fulfilled the above stated criteria.

Imaging:

Both imaging protocols comprised high-resolution T2-weighted sequences and sagittal 2D phase-contrast MRI sequences covering the entire cervical spine. Further details of imaging protocols and the different processing methods have been reported separately (Hupp et al., 2019, 2021; Pfender et al., 2022; Wolf et al., 2021; Wolf et al., 2021). Key features were summarized in Table 1.

The main differences between the two cardiac-gated phase-contrast MRI protocols between Center 1 and Center 2 were: retrospective, peripheral pulse gating using a finger-pulse oximeter versus prospective ECG-triggering, V_{ENC} gradient (2 cm/s versus 5 cm/s), time-resolution versus ≈40 timepoints per heartbeat, depending on the heart rate), and direction in which velocities were measured (caudo-cranial versus cranio-caudal), respectively.

Data processing differed by manual segmentation versus fully automated segmentation based on a trained convolutional neural network (CNN) algorithm. This led to differences regarding the size of the region of interest (ROI): standardized (manual processing, Center 1) versus variable size of the ROI that depended on the actual size of the spinal

Table 1
MRI sequences and processing techniques.

		Center 1 (Hupp et al., 2021) (Hupp et al., 2019)	Center 2 (Wolf et al., 2021) (Wolf et al., 2021)
Scanner		3 T, Siemens, MAGNETOM Skyra and Prisma	3 T, Siemens, MAGNETOM Prisma
T2-weighted sequence	Spatial resolution	$0.5 \times 0.5 \times 3\ mm^3$	$0.64 \times 0.64 \times 1.0\ mm^3$
Sagittal phase-contrast sequence	V_{ENC}	2 cm/s	5 cm/s, PEAK-GRAPPA acceleration (Jung et al., 2008)
	Direction of velocity measurements	Caudo-cranial	Cranio-caudal
	Spatial resolution	$0.4 \times 0.4 \times 5.0\ mm^3$	$0.62 \times 0.62\ mm^2 \times 3$ mm
	Cardiac gating	Retrospective pulse-trigger by finger-pulse oximeter	Prospective ECG-trigger
	Time-resolution per heartbeat	20, interpolated	≈40
Processing	Segmentation	manual	Automated, CNN-based
	Region of interest	Standard size: $20.03\ mm^2$	size varying (≈40 mm^2)*
	Angle-correction	Yes, manual	Yes, automated
	Phase-drift correction	Subtraction of the mean velocity from each single value	Point-by-point-subtraction of velocities measured in static tissue phase at the same level

*region of interest included all voxels with a CNN-based probability of ≥ 80 % to belong to spinal cord tissue at segment.

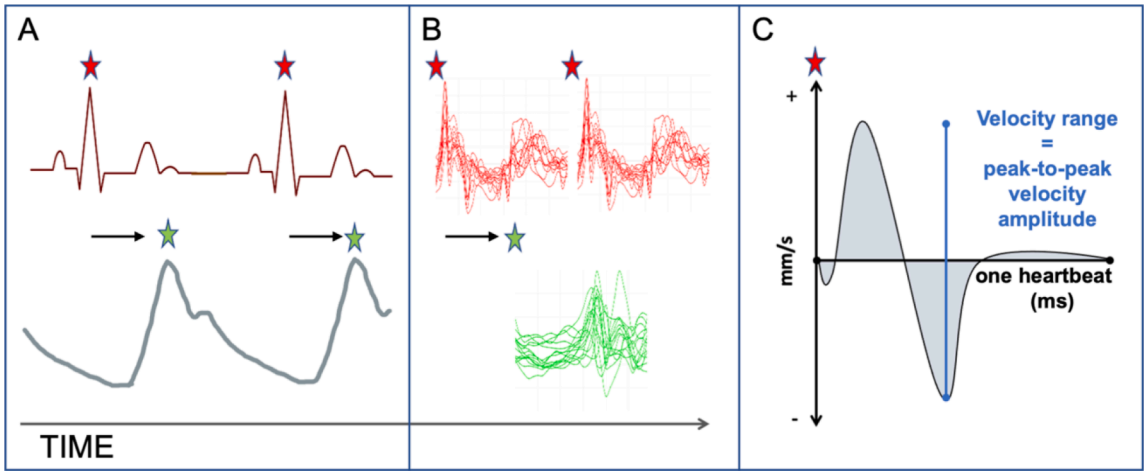

Fig. 1. Demonstration of cardiac triggering and shift of the time-resolved velocity curves. A: Cardiac-gating can be performed by ECG-triggering (red stars, R-peak, top) or peripheral finger-pulse-triggering by pulse-oximeter (green stars, pulse peak, bottom). Thus, data acquisition begins at different time-points of the cardiac cycle. B: data plots of spinal cord velocity curves over one heartbeat, red curves are ECG-triggered, green curves are triggered by peripheral finger-pulse. The main craniocaudal spinal cord motion occurs therefore at different timepoints of the recordings. To compare data, the time axis must be shifted accordingly (black arrow). C: Schematic plot of a spinal cord velocity curve measured in mm/s (y-axis) over the duration of a heartbeat measured in ms (x-axis). The velocity range (peak-to-peak velocity amplitude (mm/s)) is the difference between the maximum velocity in the caudal direction (positive value) and the maximum velocity in the cranial direction (negative value). (For interpretation of the references to colour in this figure legend, the reader is referred to the web version of this article.)

cord (automated processing, Center 2). In addition, phase-drifts were addressed differently; Center 1 subtracted the mean velocity, while Center 2 used automated point-to-point subtraction of static tissue phase. Both processing protocols applied an approximate correction by dividing by the cosine of the angle between the midline of the spinal cord and the straight, in-plane direction of the velocity measurements (manual vs automated assessment of the angle). At Center 2, an automated correction of aliasing artifacts was included within the pipeline (Herráez et al., 2002; Kasim, 2017).

Each center has evaluated and reported good to excellent interrater reliability, and scan-rescan reliability prior to this evaluation (Wolf et al., 2021; Hupp et al., 2019).

For comparison of phase-contrast MRI processing methods, the automated CNN-based pipeline (https://www.nora-imaging.org, (nora-imaging)) was adapted to data of Center 1. The CNN trained and successfully implemented at Center 2 did not sufficiently depict spinal cord tissue across the entire cervical canal in magnitude images of Center 1. Anatomical CNN-based analysis could be transferred without loss of sensitivity (rated by Dice coefficient) and used as an overlay among those cases with matching T2-weighted and phase-contrast images. Thus, further data processing including automated generation of ROIs, correction for phase-drift, angular tilt, and phase-wrapping, was identical to the processing method by Center 2.

For visualization of the velocity curves over one heartbeat (independent of its intraindividual duration and independent of different time-resolution), time-resolved velocity-plots were generated by interpolation of each dataset to 30 timepoints (Fig. 1). The plots were adapted to reflect the same caudocranial direction. It is important to note that, due to different triggering (ECG versus peripheral finger-pulse), the time-axis is shifted due to a delay between the R-peak of the ECG and the arrival of the peripheral pulse peak (Fig. 1).

For anatomical measurements of the cervical spinal canal based on the T2-weighted images, all datasets were processed by the CNN-based automated pipeline implemented in the software NORA (Wolf et al., 2021).

Parameters of interest:

The quantitative measurement made from the spinal cord velocity curve was the velocity range (peak-to-peak velocity amplitude, mm/s) per segment C2/C3 to C7/T1. This parameter is robust to phase drifts. (Fig. 1).

The anatomical parameter of interest was the adapted maximum canal compromise (aMCC) per segment (Wolf et al., 2021; Nouri et al., 2016) as a relative measure of the spinal canal narrowing calculated using the canal cross-sectional area (mm^2) per intervertebral segment C2/C3 to C7/T1 in relation to the canal cross-sectional areas one segment above and below. The higher the value, the more pronounced is the relative spinal narrowing.

2.1. Statistical analysis:

Statistical analysis was performed using IBM SPSS Statistics® Version 28.0 (IBM Corporation, IBM SPSS Statistics for Macintosh, Armonk, New York, USA). Data were given as mean and standard deviation (SD) unless otherwise indicated. Comparison of unrelated data

Table 2
Study population, and anatomical data of the spinal canal.

		Healthy participants			DCM patients		
		Center 1	Center 2	p	Center 1	Center 2	p
Number		13	13		12	12	
% Women		54	54		33	33	
Age (years)		64 ± 6	63 ± 5	0.762	51.4 ± 7	51.9 ± 13	0.786
Adapted Maximum canal compromise (aMCC)	C2/C3	1.01 ± 0.1	1.00 ± 0.1	0.727	1.02 ± 0.1	1.03 ± 0.1	0.169
	C3/C4	1.13 ± 0.1	1.11 ± 0.1	0.650	1.07 ± 0.2	1.11 ± 0.1	0.027
	C4/C5	1.04 ± 0.1	1.12 ± 0.1	0.029	1.12 ± 0.3	1.46 ± 0.6	0.449
	C5/C6	1.09 ± 0.2	1.21 ± 0.1	0.005	1.44 ± 0.4	1.75 ± 0.7	0.449
	C6/C7	1.05 ± 0.1	1.12 ± 0.1	0.022	1.12 ± 0.2	1.10 ± 0.1	0.109
	C7/T1	1.06 ± 0.1	1.05 ± 0.1	0.153	1.02 ± 0.1	1.11 ± 0.2	0.740

Table 3
Spinal cord velocity range (=peak-to-peak velocity amplitude) per heartbeat.

MRI sequence		Center 1 (V_{ENC} 2 cm/s, lower time-resolution)		Center 2 (V_{ENC} 5 cm/s, higher time-resolution)		p
MRI processing		manual		automated		
Velocity range (mm/s)	segment	mean	SD	mean	SD	
Healthy participants, n = 13	C2/C3	2.59	0.8	6.60	1.8	<0.001
	C3/C4	2.94	0.8	7.04	2.6	<0.001
	C4/C5	3.45	0.8	8.03	2.8	<0.001
	C5/C6	3.85	1.0	7.28	2.7	<0.001
	C6/C7	3.64	0.9	7.25	2.4	<0.001
	C7/T1	3.29	0.9	7.25	2.4	<0.001
Patients, n = 2	C2/C3	3.98*	2.0	7.45	2.6	0.002
	C3/C4	5.81	4.5	10.66*	3.4	0.007
	C4/C5	8.04**	6.0	13.88**	5.9	0.023
	C5/C6	10.54**	4.7	14.13**	6.9	0.260
	C6/C7	7.42**	3.1	11.71**	4.5	0.019
	C7/T1	4.85	2.6	8.50	4.6	0.027

Significant differences between healthy participants and DCM patients are indicated by asterisks (*p < 0.05, **p < 0.01).

was conducted via Mann-Whitney-*U* test. Rating reliability of different processing methods was determined via the Intra-class Correlation Coefficient (ICC, single measures, two-way mixed effect model, absolute agreement) and classified as "poor" for <0.5, "moderate" for 0.50 to 0.74, "good" for 0.75 to 0.9, and "excellent" for >0.9 (Koo and Li, 2017). Additionally, the bivariate linear relation of data was qualitatively investigated by scatter plots, and statistically by the Pearson correlation coefficient (r). Correlation was rated as "moderate" for 0.4–0.69, "strong" for 0.7 to 0.89, and "very strong" for >0.9 (Schober et al., 2018). P < 0.05 was required to assume significance.

3. Results

3.1. Study population, anatomical data and spinal cord motion data as reported by each Center

25 datasets, 12 of DCM patients and 13 of healthy participants, were identified at Center 1 and matched to 25 datasets of Center 2 (Table 2). Each DCM cohort consisted of four patients with relevant monosegmental stenosis at C4/C6 and eight with stenosis at C5/C6. At Center 1, six additional re-scans of healthy participants were eligible for automated processing, resulting in a total of 31 identically acquired datasets from Center 1 undergoing manual and automated processing.

Among healthy participants, relative spinal canal narrowing was slightly increased at the C4/C5 to C6/C7 segments in the population from Center 2 compared to that from Center 1 (Table 2, e.g., aMCC C5/C6 1.09 ± 0.2. 1.21 ± 0.1. p = 0.005). In DCM patients, there was no difference in the extent of stenosis between the two Centers (Table 1, e.g., aMCC segment C5/C6: 1.44 ± 0.4, 1.75 ± 0.7, p = 0.449), whereas the aMCC of the adjacent segment C3/C4 was higher in patients from Center 2 (aMCC 1.07 ± 0.2, 1.11 ± 0.1, p = 0.027).

The range of the spinal cord velocities in healthy participants and DCM patients were about a factor of two higher at Center 2 compared to Center 1 (Table 3, e.g., *C2*/C3: healthy participants – 2.59 ± 0.3 mm/s, 6.60 ± 1.8 mm/s, p < 0.001, DCM patients – 3.98 ± 2.0 mm/s, 7.25 ± 2.4 mm/s, p = 0.002).

At each center, DCM patients showed significantly higher spinal cord velocity ranges at the stenotic and adjacent segments compared to healthy participants (Table 3, Fig. 2, e.g., C5/C6: Center 1 – 3.85 ± 1.0 mm/s, 10.54 ± 4.7 mm/s, p < 0.001. Center 2 – 7.28 ± 2.7 mm/s, 14.13 ± 6.9 mm/s, p = 0.002).

3.2. Comparison of identically processed data (fully automated, point-to point phase-drift correction by subtraction of static tissue data)

Plots of the craniocaudal spinal cord velocity values standardized over one heartbeat showed a similar pattern, independent of the acquisition method (Fig. 3). Shortly after the beginning of the cardiac systole, a craniocaudal oscillation could be observed, followed by a second, smaller oscillation. In healthy participants, peaks are consistently steep and pronounced within measurements recorded by the phase-contrast MRI sequence of Center 2 (about 40 measurements per cardiac cycle; V_{ENC} 5 cm/s, prospective ECG-triggering). However, peaks were less pronounced and smaller within the measurements conducted by Center 1 (V_{ENC} 2 cm/s, 20 timepoints per cardiac cycle, retrospective finger-pulse-triggering). In patients, the spinal cord velocity pattern showed extensively increased craniocaudal oscillations compared to healthy participants, while peaks reached similar heights at the stenotic segments regardless of the acquisition method (Fig. 3).

The slopes of the measurements at Center 2 appear "noisier" compared to measurements at Center 1. The offset error seems less well corrected in MRI measurements from Center 1, and at lower cervical segments in measurements by Center 2 applying the automated, point-

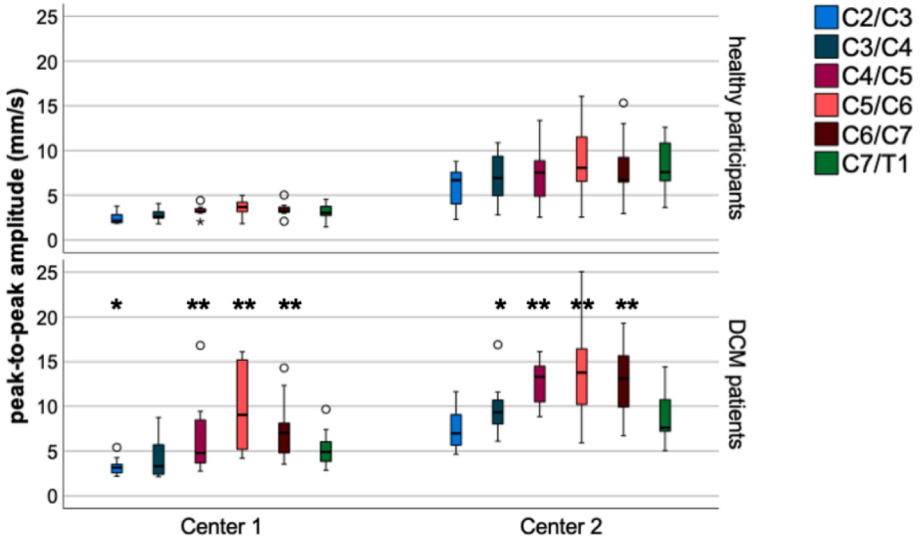

Fig. 2. Boxplots of the spinal cord velocity range (=peak-to-peak veocity amplitude) per segment measured at Center 1 and Center 2. Asterisks indicate significant differences between healthy participants and patients per Center: * p < 0.05, ** p < 0.01.

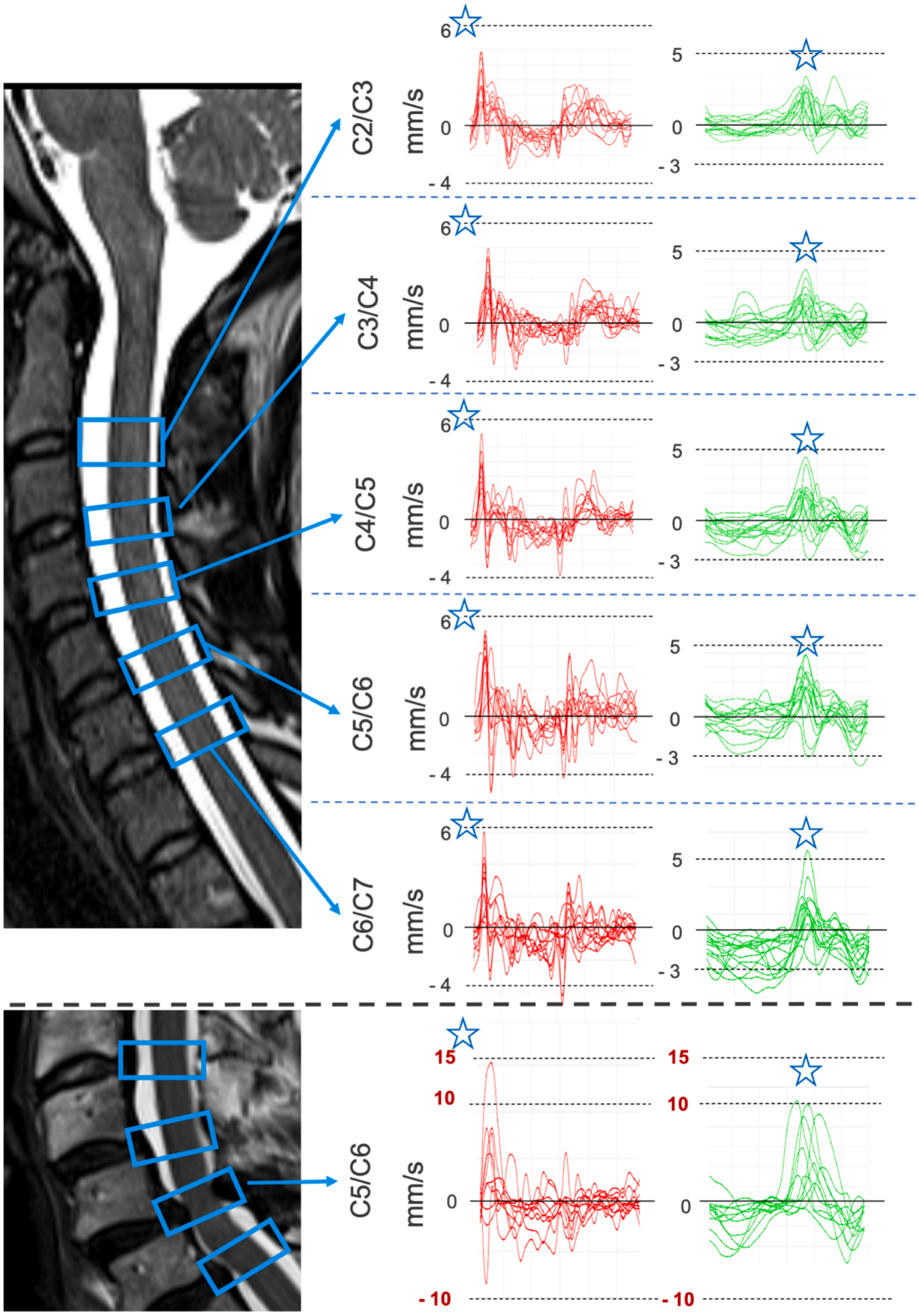

Fig. 3. Spinal cord velocities in mm/s (y-axis) as recorded by Center 1 (green curves, peripheral finger-pulse triggering) and Center 2 (red curves, ECG-triggering), processed per each intervertebral segment over one heartbeat (x-axis). Positive values represent motion in the caudal direction, and negative values in the cranial direction. At the top, measurements of 13 matched healthy participants are displayed. An early craniocaudal peak at the beginning of the cardiac cycle (blue star) can be observed within all measurements (time variation due to different method of cardiac gating, see Fig. 1). At the bottom, measurements at segment C5/C6 of all DCM patients presenting with stenosis at C4/C5 or C5/C6 are plotted. Note the increased range of spinal cord velocity on the y-axis. (For interpretation of the references to colour in this figure legend, the reader is referred to the web version of this article.)

Table 4
Rating reliability of two different processing pipelines generating the spinal cord velocity range (=peak-to-peak velocity amplitude) of identically acquired spinal cord velocity curves; ICC – Intra-class Correlation Coefficient, r – Pearson correlation coefficient.

	segment	ICC	p	*r*	p
Velocity range (peak-to-peak velocity amplitude)	C2/C3	0.890	<0.001	0.758	<0.001
	C3/C4	0.862	<0.001	0.880	<0.001
	C4/C5	0.992	<0.001	0.981	<0.001
	C5/C6	0.991	<0.001	0.944	<0.001
	C6/C7	0.921	<0.001	0.821	<0.001
	C7/T1	0.739	<0.001	0.650	<0.001

by-point correction of Center 2.

A quantitative comparison of identically processed data between Centers reproduced similar results among healthy participants and DCM patients, with significantly higher values at Center 2 compared to Center 1 (Supplement 2).

3.3. Comparison of different processing techniques (identical MRI sequences, automated versus manual processing)

The rating reliability of the two processing methods to assess the velocity range was excellent at segments C4/C5 to C6/C7 (>0.9), good at segment C2/C3, and C3/C4 (ICC > 0.8), and moderate at segment C7/T1 (ICC 0.739, Table 4). Scatter plots and correlation analysis (Fig. 4, Table 4) showed a strong linear relationship between the spinal cord velocity range generated by the two different processing methods, with the best results at segments C4/C5 and C5/C6 (r > 0.9); the correlation at segment C7/T1 was moderate (r = 0.650, p > 0.001). For further visualization, additional Bland-Altmann plots per segment can be found in Supplement 2.

4. Discussion

This study presents an evaluation of different phase-contrast MRI sequences and processing techniques to assess cervical spinal cord motion across two centers. Analysis demonstrated a genuine spinal cord motion pattern per heartbeat and a pathologically increased spinal cord motion in DCM patients (e.g., extensively increased oscillations, Fig. 3), which was depicted by different techniques. Differences between spinal cord velocity ranges may mainly be attributed to different time-resolution used for phase-contrast MRI sequences. Sufficient time-resolution (approximately >20 true timeframes per heartbeat) will be important to depict the physiological range of spinal cord motion. Until further explorations of a sufficient lower limit, the maximum operable time-resolution should be aimed for. Manual versus automated processing techniques appeared to equivalent results, while the application of standardized CNN-based protocols across Centers would benefit from identical MRI sequences.

Acquisition of phase-contrast MRI data:

The spinal cord motion pattern revealed very prominent peaks of spinal cord motion at the beginning of the cardiac cycle across both acquisition techniques and centers. In a setting of higher time resolution, the peaks were reproducibly higher and steeper in comparison to those in lower time-resolution assessments (Fig. 3). This phenomenon can be physically explained: the sensitivity to depict a short period of motion increases with higher time resolution, and the true peaks are more likely to be resolved. This explains the main differences across centers in spinal cord motion analysis. Major disparities were observed within healthy participants (physiologically lower velocity ranges), whereas assessments of pathologically increased spinal cord motion in DCM patients was similar. Thus, a setting of low time-resolution leads to a systematic underestimation of velocity values. Retrospective gating may have an additional effect: in retrospective triggering, data were interpolated and therefore the technique might be slightly less sensitive to short and smaller peaks at a certain timepoint (Lotz et al., 2002). Also, higher V_{ENC} might cause a slightly greater data variability (Lotz et al., 2002).

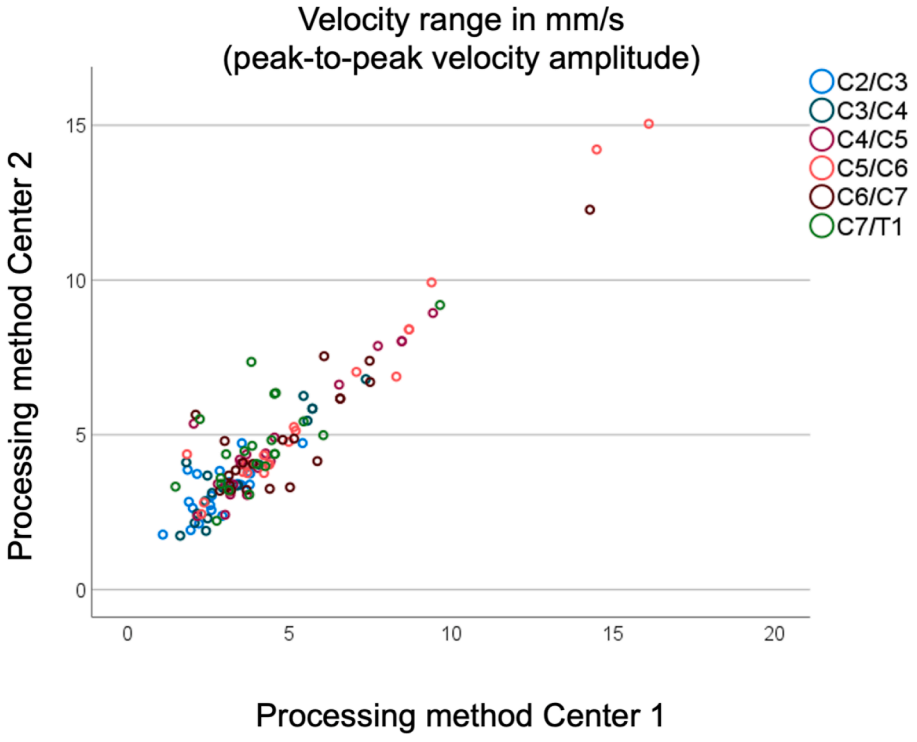

Fig. 4. Scatter plot of different processing methods of 31 identically acquired phase-contrast MRI measurements: data were processed by a manual method of Center 1 (x-axis) and by a fully automated pipeline (Center 2, y-axis). The spinal cord velocity range (peak-to-peak-velocity amplitude) in mm/s was generated; data show a strong linear relation at all segments (r > 0.76) except at C7/T1 (r = 0.65).

Overall, the effects of these differences across the MRI protocols are expected to be weak.

It would need further exploration within larger trials to determine whether the low time-resolution setting can depict relevantly increased spinal cord motion at a sufficient level of sensitivity.

Processing of phase-contrast MRI data:

The velocity range (peak-to-peak velocity amplitude) has been reliably depicted by both processing methods, making it attractive for possible clinical implementation.

Data processing was less reliable at segment C7/T1, which had already been observed by intra-center analysis of Center 1 previously (Hupp et al., 2019), while data reproducibility had been good at the same segment at Center 2 (Wolf et al., 2021). Thus, we conclude that this effect is more likely attributed to the MRI technique than to the processing. Possible confounding factors could be the applied coil, slight tilt of the sagittal plane, or artifacts caused by the arch of the aorta.

Other useful measurements that can be made from the velocity curves, such as the total displacement of the spinal cord over one heartbeat, might be less reliable as it is sensitive to phase-drifts. This parameter might be used with caution in a setting of identical scanners, order of MRI sequences, and processing. Additionally, it should be noted that differences in cardiac gating could have a small but possibly important impact, as prospective gating causes minor measurements gaps at the end of the cardiac cycle in contrast to retrospective triggering.

Current visualization of the velocity plots including a point-by-point subtraction of static tissue phase for phase-drift correction, seem to show a higher offset error in datasets of Center 1 and at lower segments measured by Center 2 (Fig. 3). In our experience, including non-published data, phase-drift correction by point-to-point subtraction of static tissue phase cannot always be reliably implemented at the cervical spine due to varying effects depending on the site, direction, and time of acquisition. A subtraction of the mean or median may give a method that is independent of these effects, and which is currently applied in ongoing trials at both centers.

One limitation of the study is the small sample size. It must be noted that slight inter-center differences of automated processing methods might have remained, as phase-contrast MRI sequences of Center 1 were not directly segmented within the magnitude images but overlayed on matching T2-weighted images. Still, the exploration detected a major cause explaining data variability while similar spinal cord motion patterns were depicted. This is an important step that underscores the authenticity of spinal cord motion and the general feasibility of its analysis. To continue with further research and clinical studies, comparisons between scanners applying identical MRI sequences and processing methods should be conducted. We see this work as a basic study upon which future potential multicenter studies can be based.

5. Conclusion

Data demonstrated a consistent and very specific pattern of physiological craniocaudal spinal cord motion in healthy participants and definite pathological increase in DCM patients across two centers. Variability of measurements were due to differences in acquisition techniques, e.g., differences in time-resolution. Diagnostic studies should aim for a maximum achievable time-resolution to depict the entire range of spinal cord motion.

Focusing on the velocity range (which is equivalent to the peak-to-peak velocity amplitude) is recommended, as the value is easy to generate, robust to different methods of processing, and not affected by phase-drift. Automated segmentation and processing will enable unbiased, consistent, time-saving, and uniform analysis.

CRediT authorship contribution statement

Katharina Wolf: Conceptualization, Methodology, Software, Investigation, Validation, Resources, Data curation, Visualization, Project administration, Funding acquisition, Writing – original draft. **Nikolai Pfender:** Conceptualization, Methodology, Investigation, Validation, Resources, Data curation, Writing – review & editing. **Markus Hupp:** Conceptualization, Methodology, Investigation, Validation, Resources, Data curation, Project administration, Writing – review & editing. **Marco Reisert:** Conceptualization, Software, Methodology, Validation, Resources, Writing – review & editing. **Axel Krafft:** Conceptualization, Software, Methodology, Validation, Resources, Writing – review & editing. **Reto Sutter:** Conceptualization, Resources, Writing – review & editing. **Marc Hohenhaus:** Investigation, Resources, Data curation, Writing – review & editing. **Horst Urbach:** Resources, Writing – review & editing. **Mazda Farshad:** Resources, Writing – review & editing. **Armin Curt:** Conceptualization, Methodology, Investigation, Validation, Resources, Data curation, Project administration, Funding acquisition, Writing – review & editing.

Declaration of Competing Interest

The authors declare that they have no known competing financial interests or personal relationships that could have appeared to influence the work reported in this paper.

Data availability

Data will be made available on request.

Acknowledgements

We would like to thank all healthy volunteers and patients for participation in this study.

Appendix A. Supplementary data

Supplementary data to this article can be found online at https://doi.org/10.1016/j.nicl.2023.103334.

References

Bradley, W.G., Haughton, V., Mardal, K.A., 2016. Cerebrospinal fluid flow in adults. Hand. Clin. Neurol. 135, 591–601.

Bunck, A.C., Kroger, J.P., Juttner, A., Brentrup, A., Fiedler, B., et al., 2011. Magnetic resonance 4D flow characteristics of cerebrospinal fluid at the craniocervical junction and the cervical spinal canal. Eur. Radiol. 21, 1788–1796.

Carroll, I., Callen, A., 2022. Phase contrast spina MRI for the evaluation of CSF leak, and why it matters. Neurology. https://doi.org/10.1212/WNL.0000000000201694.

Chank, H.S., Neja, T., Yoshida, S., et al., 2014. Increased flow signal in compressed segments of the spinal cord in patients with cervical spondylotoc myelopathy. Spine 39, 2136–2142.

Cushing, H., 1925. The third circulation and its channels. (Camerun lecture). Lancet 2, 851–857.

Davies, B.M., Mowforth, O., Gharooni, A.A., Tetreault, L., Nouri, A., Dhillon, R.S., Bednarik, J., Martin, A.R., Young, A., Takahashi, H., Boerger, T.F., Newcombe, V.F., Zipser, C.M., Freund, P., Koljonen, P.A., Rodrigues-Pinto, R., Rahimi-Movaghar, V., Wilson, J.R., Kurpad, S.N., Fehlings, M.G., Kwon, B.K., 2022. A new framework for investigating the biological basis of degenerative cervical myelopathy [AO Spine RECODE-DCM Research Priority Number 5]: mechanical stress, vulnerability and time. Global Spine J. 12 (1_suppl), 78S–96S. https://doi.org/10.1177/219256822110.

Herráez, M.A., Burton, D.R., Lalor, M.J., Gdeisat, M.A., 2002. Fast two-dimensional phase-unwrapping algorithm based on sorting by reliability following a noncontinuous path. Appl. Opt. 41 (35), 7437–7444. https://doi.org/10.1364/ao.41.007437.

Hoxworth, J.M., 2014. Measuring CSF flow dynamics in Spontaneous intracranial hypotension with phase-contrast magnetic resonance imaging: potential implications for diagnosis and treatment. Cephalgie 34 (8), 565–567.

Hupp, M., Vallotton, K., Brockmann, C., Huwyler, S., Rosner, J., Sutter, R., Klarhoefer, M., Freund, P., Farshad, M., Curt, A., 2019. Segmental differences of cervical spinal cord motion: advancing from confounders to a diagnostic tool. Sci. Rep. 9 (1), 7415. https://doi.org/10.1038/s41598-019-43908-x.

Hupp, M., Vallotton, K., Brockmann, C., et al., 2019. Segmental differences of cervical spinal cord motion: advancing from confounders to a diagnostic tool. Sci. Rep. 9 (1), 7415. https://doi.org/10.1038/s41598-019-43908-x.

Hupp, M., Pfender, N., Vallotton, K., Rosner, J., Friedl, S., Zipser, C.M., Sutter, R., Klarhöfer, M., Spirig, J.M., Betz, M., Schubert, M., Freund, P., Farshad, M., Curt, A., 2021 Mar. The restless spinal cord in degenerative cervical myelopathy. AJNR Am. J. Neuroradiol. 42 (3), 597–609.

Johnson, K.M., Markl, M., 2010. Improved SNR in phase contrast velocimetry with five-point balanced flow encoding. Magn. Reson. Med. 63, 349–355.

Jung, B., Ullmann, P., Honal, M., Bauer, S., Hennig, J., Markl, M., 2008. Parallel MRI with extended and averaged GRAPPA kernels (PEAK-GRAPPA): optimized spatiotemporal dynamic imaging. J. Magn. Reson. Imaging 28 (5), 1226–1232.

Kasim, M.F. 2017. "Fast 2D phase unwrapping implementation in MATLAB", https://github.com/mfkasim91/unwrap_phase/. GitHub. [Online] GitHub Inc., 03 28, 2022. [Cited: 11 03, 21.] https://github.com/mfkasim1/unwrap_phase.

Kelly, E.J., Yamada, S., 2016. Cerebrospinal fluid flow studies and recent advancements. Semin. Ultrasound CT MRI 37, 92–99.

Koo, T.K., Li, M.Y. 2017. A Guideline of Selecting and Reporting Intraclass Correlation Coefficients for Reliability Research [published correction appears in J Chiropr Med. 16(4):346]. doi:10.1016/j.jcm.2016.02.012, 15(2):155-163.

Lotz, J., Meier, C., Leppert, A., Galanski, M., 2002. Cardiovascular flow measurement with phase-contrast MR imaging: basic facts and implementation. Radiographics. 22 (3), 651–671. https://doi.org/10.1148/radiographics.22.3.g02ma11651.

Markl, M. 2022. Velocity encoding and flow imaging. [Online] 12 08, 2022. [Cited: 12 08, 2022.] https://ece-classes.usc.edu/ee591/library/Markl-FlowImaging.pdf.

Matsuzaki, H., Wakabayashi, K., Ishihara, K., et al., 1996. The origin and significance of spinal cord pulsation. Spinal Cord. 34 (7), 422–428.

nora-imaging. [Online] http://www.nora-imaging.org.

Nouri, A., Martin, A.R., Mikulis, D., Fehlings, M.G., 2016. Magnetic resonance imaging assessment of degenerative cervical myelopathy: a review of structural changes and measurement techniques. Neurosurg Focus. 40 (6), E5. https://doi.org/10.3171/2016.3.FOCUS1667 [Online],.

Pfender, N., Rosner, J., Zipser, C.M., Friedl, S., Vallotton, K., Sutter, R., Klarhoefer, M., Schubert, M., Betz, M., Spirig, J.M., Seif, M., Hubli, M., Freund, P., Farshad, M., Curt, A., Hupp, M., 2022. Comparison of axial and sagittal spinal cord motion measurements in degenerative cervical. J. Neuroimaging. https://doi.org/10.1111/jon.13035. Epub ahead of print.

Schmidt, R.M., Bauer, H., Hanzal, F., Lowenthal, A., Schabinski, G., Frick, W., Linke, P. G., Quadbeck, G. 1968. Der Liquor cerebrospinalis. Untersuchungsmethoden und Diagnostik. [ed.] Rudolf Manfred Schmidt. Berlin: VEB Verlag Volk und Gesundheit,.

Schober, P., Boer, C., Schwarte, L.A., 2018. Correlation coefficients: appropriate use and interpretation. Anesth. Analg. 126 (5), 1763–1768. https://doi.org/10.1213/ANE.0000000000002864.

Stöcklein, S.M., Brandlhuber, M., Lause, S.S., Pomschar, A., Jahn, K., Schniepp, R., Alperin, N., Ertl-Wagner, B., 2022. Decreased craniocervical CSF flow in patients with normal pressure hydrocephalus: a pilot study. AJNR Am. J. Neuroradiol. 43 (2), 230–237. https://doi.org/10.3174/ajnr.A7385.

Tain, R.W., Bagci, A.M., Byron, L.L., Sklar, E.M., Ertl-Wagner, B., Alerpin, N., 2011. Determination of cranio-spinal canal compliance distribution by MRI: methodology and early application in idiopathy intracranial hypertension. J. Magn. Reson. Imaging 34 (6), 1397–1404.

Vavasour, I.M., Meyers, S.M., MacMillan, E.L., et al., 2013. Increased spinal cord movements in cervical spondylotic myelopathy. Spine J. 14 (10), 2344–2354.

Wolf, K., Reisert, M., Beltran, S., Klingler, J.H., Hubbe, U., Egger, K., Krafft, A.J., Hohenhaus, M. 2021. Focal cervical spinal stenosis causes mechanical strain on the entire cervical spinal cord tissue – a prospective controlled, matched-pair analysis applying phase-contrast MRI. NeuroImage:Clinical epub ahead of print, doi: 10.1015/j.Nicl.2021.102580.

Wolf, K., Luetzen, N., Elsheikh, S., Reisert, M., Beltran, S., Kremers, N., Fung, C., Beck, J., Urbach, H. 2022. Abstract 754 - Rückenmarkbewegung bei spontaner idiopathischer Hypotension, idiopathischer intrakranialler Hypertension und Gesunden: ein neues Target? DGN, http://ebook.dgnvirtualmeeting.org/#480.

Wolf, K., Krafft, A., Egger, K., Klingler, J.H., Hubbe, U., Reisert, M., Hohenhaus, M., 2019. Assessment of spinal cord motion as a new diagnostic MRI-parameter in cervical spinal canal stenosis: study protocol on a prospective longitudinal trial. J. Orthop. Surg. Res. 14 (1), 321. https://doi.org/10.1186/s13018-019-1381-9.

Wolf, K., Reisert, M., Beltrán, S.F., Klingler, J.H., Hubbe, U., Krafft, A.J., Kremers, N., Egger, K., Hohenhaus, M., 2021. Spinal cord motion in degenerative cervical myelopathy: the level of the stenotic segment and gender cause altered pathodynamics. J. Clin. Med. 10 (17), 3788. https://doi.org/10.3390/jcm10173788.

Wolf, K., Luetzen, N., Mast, H., Kremers, N., Reisert, M., Beltrán, S., Fung, C., Beck, J., Urbach, H., 2022. CSF flow and spinal cord motion in patients with spontaneous intracranial hypotension: a phase contrast MRI study. Neurology. https://doi.org/10.1212/WNL.0000000000201527.

Wymer, D.T., Patel, K.P., Burke 3rd, W.F., Bhatia, V.K., 2020. Phase-contrast MRI: physics, techniques, and clinical applications. Radiographics. 40 (1), 122–140. https://doi.org/10.1148/rg.2020190039.